Electronic Supplementary Information

Nanoscale, conformal polysiloxane thin film electrolytes for three-dimensional battery architectures

Nan Chen[†, a], B. Reeja-Jayan[†, a], Jonathan Lau[b], Priya Moni[c], Andong Liu[a], Bruce Dunn[b], Karen K. Gleason*[, a]

Table S1. iCVD deposition conditions for PV4D4 film growth

Depositions	$T_{substrate}$ [°C]	$T_{filament}$ [°C]	V4D4 flow rate [sccm][b]	TBPO flow rate [sccm]	P_m/P_{sat} [a]	Average film deposition rate [nm min^{-1}]
1	45	300	0.15	1.0	0.50	0.90
2	35	300	0.15	1.0	0.50	1.2
3	30	300	0.15	1.0	0.50	1.4
4	25	300	0.15	1.0	0.50	1.7
5	35	300	0.15	1.0	0.95	1.8
6	35	300	0.15	1.0	0.30	0.72

[a)] P_m/P_{sat} defines monomer saturation ratio, which presents the effective surface concentration of the monomer on the substrate surface at the start of film growth.

[b)] sccm stands for standard cubic centimeters per minute

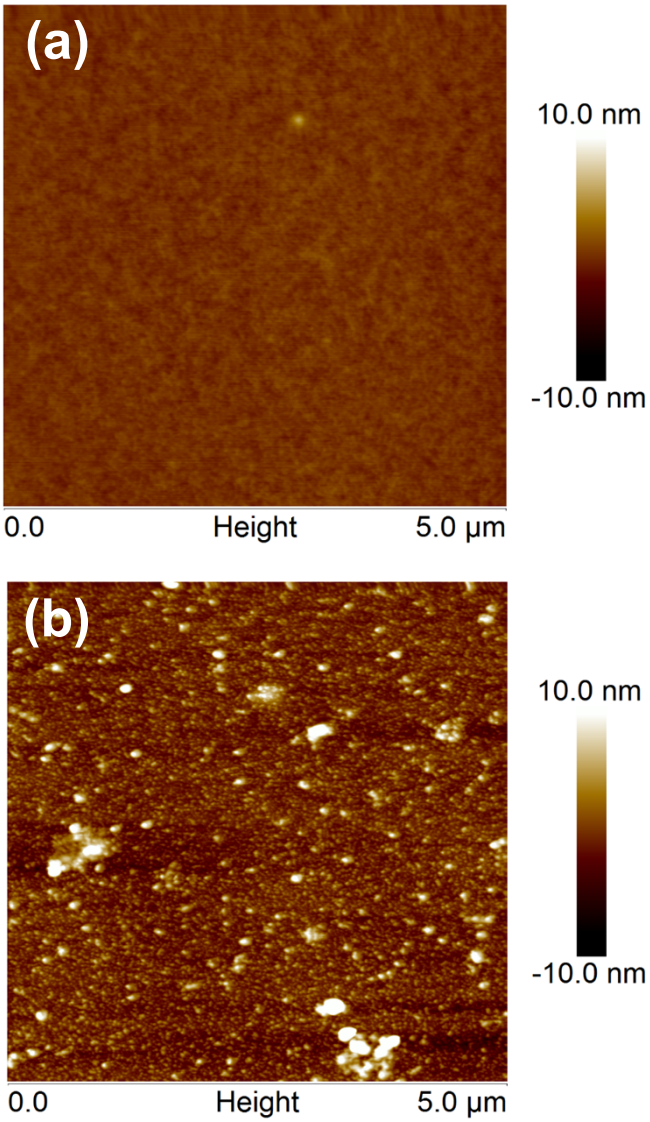

Figure S1: a) AFM image of iCVD deposited 35 nm PV4D4 film on silicon wafer (R_{rms} = 0.463); b) AFM image of the same PV4D4 film after lithiation (R_{rms} = 2.20 nm). R_{rms} is the root mean square roughness. Energy dispersive x-ray spectroscopy (EDS) in scanning electron microscope (SEM) reveals that the clusters contain Cl suggesting the presence of $LiClO_4$ clusters. Work to elucidate the exact role of these clusters on ionic conductivity is ongoing.

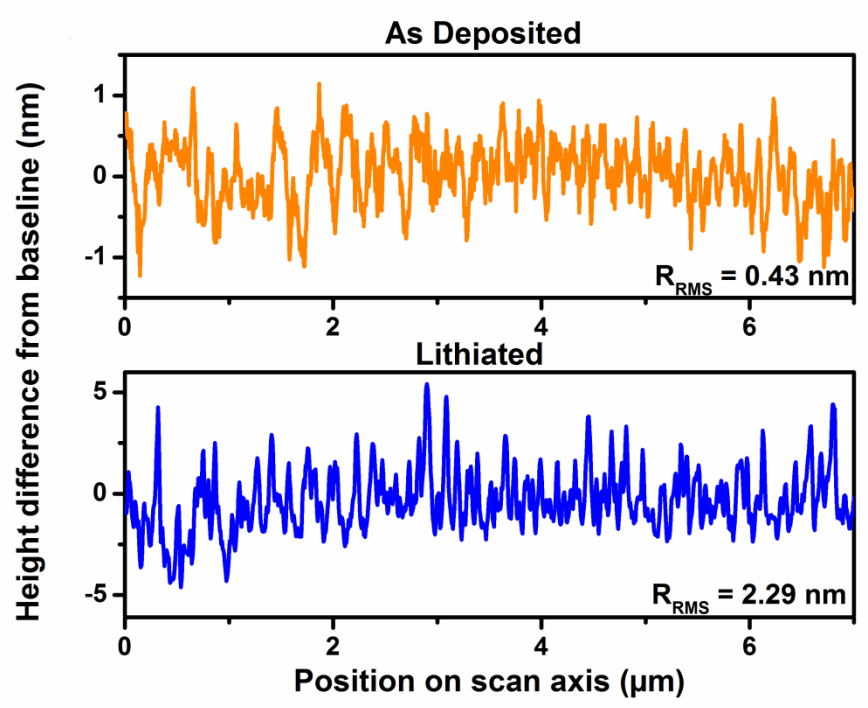

Figure S2: AFM line scans measured across the center of AFM images in Figure S1a (as deposited) and Figure S1b (Lithiated)

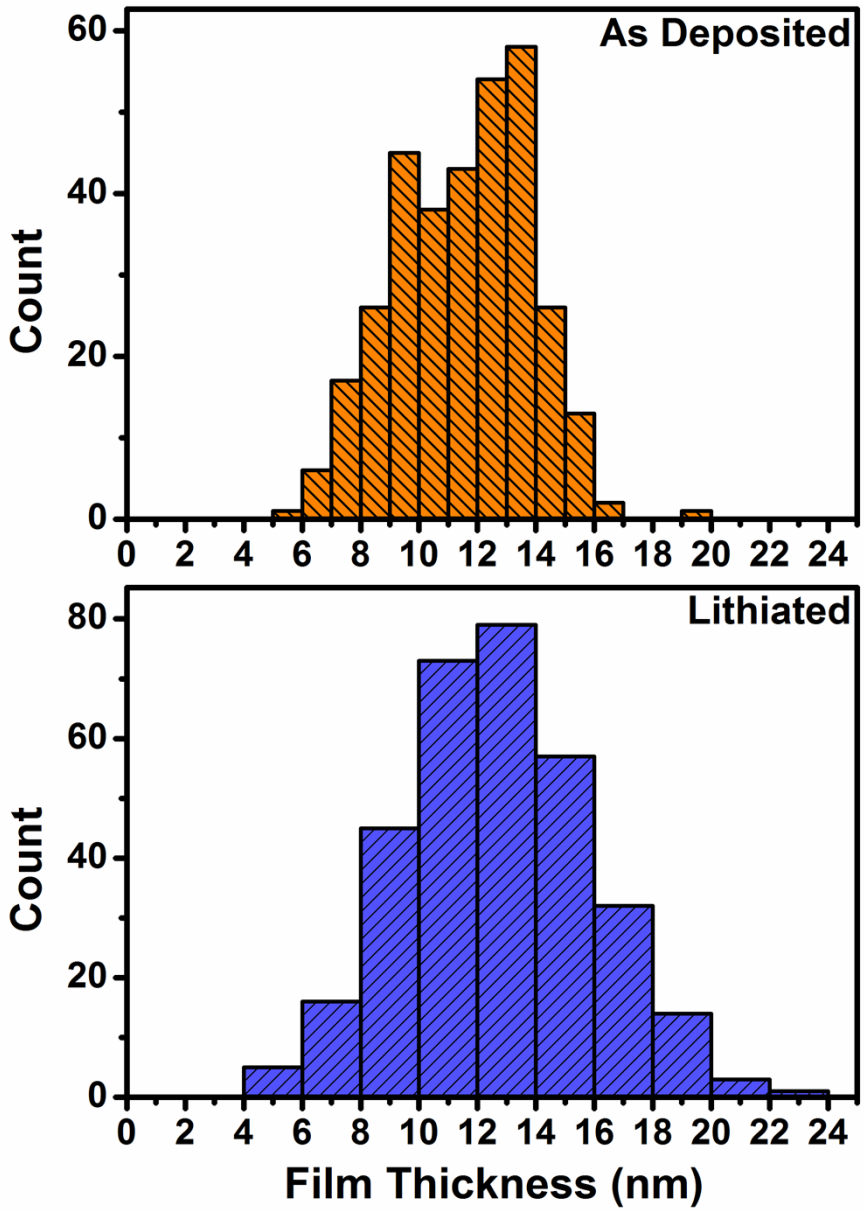

Figure S3: Comparison of PV4D4 film thickness distribution for as deposited and lithiated PV4D4 coated Ag nanowires, based on TEM imaging. The mean thickness and standard deviation of the as deposited film are 11.5 nm and 2.6 nm respectively. After lithiation, there is a marginal increase in mean thickness and standard deviation to 12.6 nm and 3.2 nm respectively. To obtain the data, 11 wires were chosen at random from different locations of the grid and 30 measurements were taken on each wire for both the as deposited and lithiated samples.

Table S2. Comparison of PV4D4 film thickness on silicon wafer before and after lithiation obtained from VASE. Both film thickness and mean squared error (MSE), which represents film roughness, show marginal changes after soaking in Li salt solution for 3 days. MSE values are typically around 4~5 for extremely smooth surfaces like polished silicon.

Positions	PV4D4 before soaking in Li salt solution		PV4D4 after soaking in Li salt solution	
	Thickness [nm]	MSE	Thickness [nm]	MSE
1	35.9	5.2	36.8	5.5
2	36.0	5.0	37.1	5.0
3	36.0	4.9	36.9	5.1
4	35.5	4.1	36.8	4.6
5	35.9	4.8	36.7	5.3
Averaged	35.86		36.86	

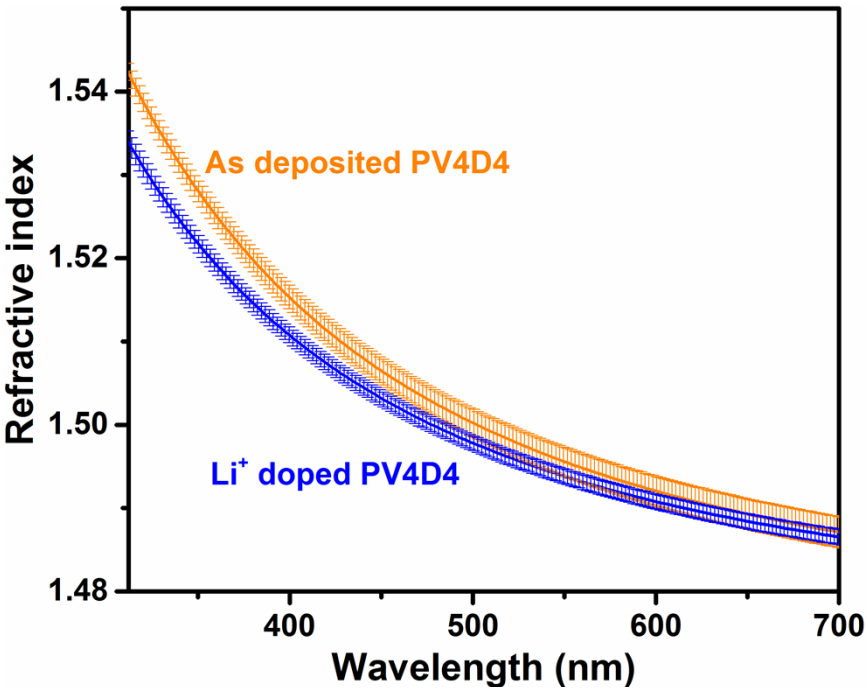

Figure S4: Comparison of refractive index of PV4D4 film on silicon wafer before and after lithiation, obtained from VASE. Refractive index of film also shows only marginal changes after soaking in Li salt solution for 3 days. Data is the average of measurements at 5 positions on the film sample. Error bars indicate deviation from this average value.

Electrical and Impedance Measurements

The electronic and ionic conductivities of the films were calculated using Equation 1 from the manuscript. The sample thickness is determined by VASE. The DC resistance or the ionic resistance is determined from equivalent circuit fitting, and the contact area is determined by the size of Hg electrodes. The limits of the reported conductivities were calculated using the range of possible contact areas for the Hg electrodes.

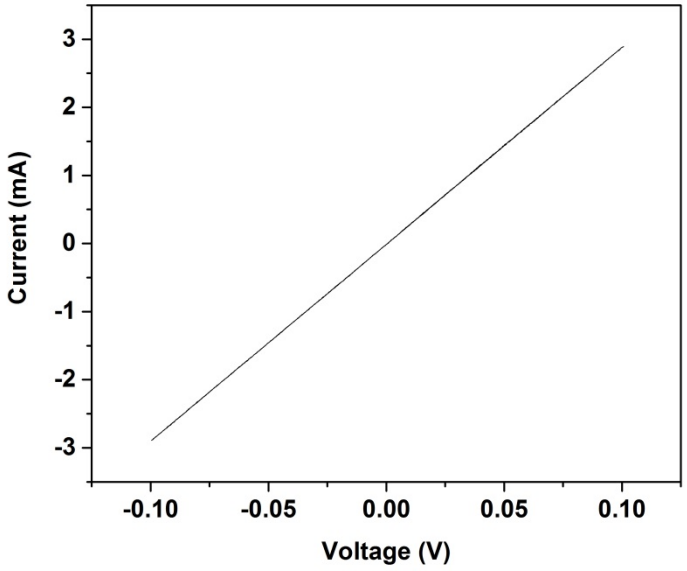

Figure S5: DC current-voltage curve of the unlithiated 25 nm PV4D4 film; the voltage range is taken with respect to the open-circuit voltage of the system at a scan rate of 2 mV s^{-1}. The current is shown to be linear and fully reversible. The unlithiated 35 nm PV4D4 film exhibited a similar impedance response.

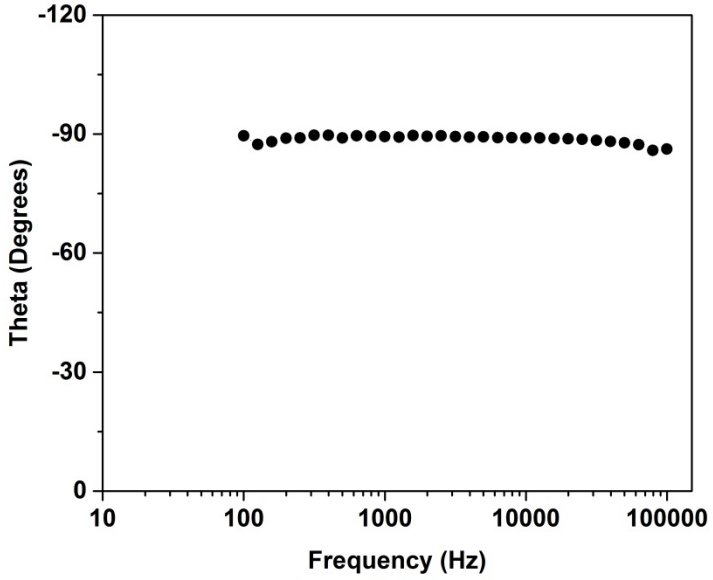

Figure S6: Frequency dependence of the phase angle for the unlithiated 25 nm PV4D4 film. The data were taken in the frequency range from 100 kHz to 100 Hz using a 10 mV (RMS) potential. The near -90˚ phase angle in this plot are consistent with the response of a dielectric material. The unlithiated 35 nm PV4D4 film exhibited a similar impedance response.

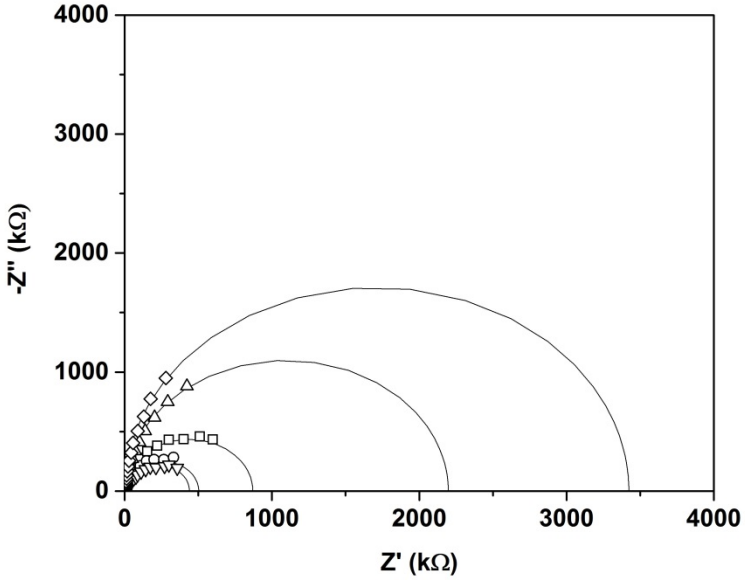

Figure S7: Impedance of the lithiated 35 nm PV4D4 films. The data were taken in the frequency range from 100 kHz to 100 Hz using a 10 mV (RMS) potential. The semi-circles are indicative of ionic conduction. The solid curves were obtained from data fitting and used to determine R_p. The higher impedance observed for thicker lithiated polymers suggests an inhomogeneous distribution of charge carriers in the film.

Table S3. Comparison of ionic conductivity among different film electrolytes. Nanoscale, conformal electrolytes are indicated by *.

Material	Deposition Method	Film Thickness [nm]	Ionic conductivity at 25°C [S cm^{-1}]	Conformal	Ref #
PV4D4*	iCVD	25	10^{-8}	Yes	Present work
PPO*	Electrodeposition	21	10^{-10}	Yes	1
PMMA*	Polymer infiltration	25-30	Not reported	Yes	2
PEO	Solution	70000	10^{-8}	No	3
LiPON	Sputtering	3000	10^{-7}	No	4
LASO*	Atomic layer deposition (ALD)	12	10^{-9}	Yes	5

iCVD PV4D4 films demonstrate the highest ionic conductivity value reported among nanoscale, conformal thin film electrolytes.

Organic electrolytes:
PV4D4 – Poly (tetravinyltetramethylcyclotetrasiloxane)
PPO - Poly (phenylene oxide)
PMMA - Poly(methyl methacrylate)
PEO - Poly (ethylene oxide)

Inorganic electrolytes:
LiPON - Lithium Phosphorus Oxynitride
LASO - Lithium Aluminum Silicate

Pinhole Characterization

Pinhole characterization was carried out using electrochemical techniques outlined in detail elsewhere.[6] If it is assumed that pinholes act as independent disk-shaped electrodes, then the approximate pinhole density can be modeled and described by Equation S1 where N is the number density of pinholes, j is the peak current density, r_0 is the average pinhole radius, F is the Faraday constant, and D and C^* are the diffusion coefficient (for a redox system with bare working electrodes) and concentration of the probe molecule, respectively.[6]

$$N = \frac{j}{4nFDC^* r_0} \quad \text{(S1)}$$

A critical parameter required in calculating the pinhole density is r_0, which must be determined independently. To this end, a pair of redox couples with different solvation shell diameters was employed to observe changes in cyclic voltammograms as a function of redox molecule size. In order to calculate and catalogue these diameters, diffusion coefficients of the redox couples, D, were first determined from voltammograms using the Randles-Sevcik equation (Equation S2), where i_p is the peak current, n is the number of electrons transferred per redox molecule, F is the Faraday constant, A is the electrode area, C is the concentration of the redox couple, v is the scan rate, and R is the gas constant. The coefficients can be extracted as the slope of peak currents versus the square root of the scan rate.[7]

$$i_p = 0.4463nFAC\left(\frac{nFvD}{RT}\right)^{\frac{1}{2}} \quad \text{(S2)}$$

The Stokes-Einstein equation (Equation S3) is then used to determine the diameter of the diffusing species, d, where k_B is the Boltzmann constant, and η is the viscosity of the solvent used in the redox system.[7,8]

$$D = \frac{k_B T}{3\pi\eta d} \quad \text{(S3)}$$

Diffusion coefficients determined from the oxidation peak currents were used in the calculations of the solvation shell diameter for consistency.

Heterogeneous rate constants, k^0, are another useful parameter for pinhole characterization because they are a measure of the difficulty for electrons to transfer from the redox molecule to the electrode. Therefore, redox couples with large k^0 values may be able to exchange electrons at defect sites that may not necessarily be accessible given the size considerations of the pinhole and probe molecule.[6] Rate constants for the redox couples were determined

through the Nicholson relationship[6] (Equation S4 and S5) where ψ is related to the voltage separation of the oxidation and reductions peaks observed from cyclic voltammetry of the redox couples, k^0 is the rate constant, D_O and D_R are the oxidation and reduction diffusion coefficients, and the other variables are consistent with previous equations.

$$\psi = \frac{\gamma^a k^0}{\sqrt{n\pi F v D_O / RT}} \quad \text{(S4)}$$

$$\gamma = \left(\frac{D_O}{D_R}\right)^{\frac{1}{2}} \quad \text{(S5)}$$

Electrochemical measurements were performed on 1 cm^2 samples of PV4D4 films deposited on ITO coated glass substrates in a three-electrode cell with platinum counter and reference electrodes. In the determination of diffusion coefficients, Pt or Au microelectrodes are often used due to several advantages over macroelectrodes, including intrinsically larger heterogeneous rate constants and the minimization of uncompensated resistance and capacitive distortion.[7,9-10] However, macroelectrodes offer better statistical data of the coating coverage and a larger signal-to-noise ratio for electrolyte-coated electrodes that demonstrate decreased currents. Because of this, a 2 cm^2 bare Pt and a 1 cm^2 ITO working electrodes were employed to validate the use of macroelectrodes in these measurements and to ensure that the calculated diffusion coefficients of dmFc and $CoCp_2PF_6$ are reflective of those reported in literature.[8,11] In some cases, the diffusion coefficients for the redox systems in PC were not available and values for the redox systems in acetonitrile (ACN) were used for comparison instead.

Diffusion coefficients determined through cyclic voltammetry for the dmFc and $CoCp_2PF_6$ redox systems with Pt working electrodes were calculated to be 1.85 x 10^{-6} and 2.21 x 10^{-6} cm^2 s^{-1}, respectively (Figure S8). These values are consistent with those reported in literature,[8,11] validating the use of macroelectrodes. Diffusion coefficients for these redox systems with bare ITO working electrodes were calculated to be 3.80 x 10^{-7} and 4.93 x 10^{-7} cm^2 s^{-1}, lower than those of Pt electrodes by approximately one order of magnitude. This effect has been observed across different electrodes in other redox systems and may be ascribed to differences in the charge transfer coefficients between Pt and ITO.[12] Using the diffusion coefficients with bare ITO working electrodes, the solvation shell diameters of dmFc and $CoCp_2PF_6$ were determined to be 4.51 and 3.48 nm, and the heterogeneous rate constants were calculated to be 2.21 x 10^{-4} and 2.66 x 10^{-4} cm s^{-1}, respectively.

Cyclic voltammetry using the dmFc and $CoCp_2PF_6$ redox systems was carried out on unlithiated and lithiated 20 nm PV4D4 films. While the $CoCp_2PF_6$ redox system was expected to result in greater peak currents due to the smaller size of the redox molecule and greater accessibility of the ITO substrate through pinholes, peak currents for the dmFc redox system were demonstrably larger (Figure S9). Because the heterogeneous rate constants of these redox systems are comparable to one another, an alternative explanation is needed to explain this discrepancy. It has been argued elsewhere that if pinholes are assumed to be in the same size regime as the probe molecules, selectivity may arise due to chemical characteristics rather than physical size of the probe molecules.[6] As such, the pinholes can be reasonably estimated as 4 nm in diameter, or a radius, r_0, of 2 nm.

The oxidation peak current densities for dmFc and $CoCp_2PF_6$ for use in equation S1 were determined at scan rates of 700 mV s^{-1}. At this scan rate, the Faradaic currents from the redox couples can be accurately decoupled from any capacitive contribution while also avoiding the significant ohmic drop or RC time constant distortion that can affect cyclic voltammograms at faster scan rates.[9] From these peak current densities, the number density of pinholes 4 nm in diameter can be calculated.

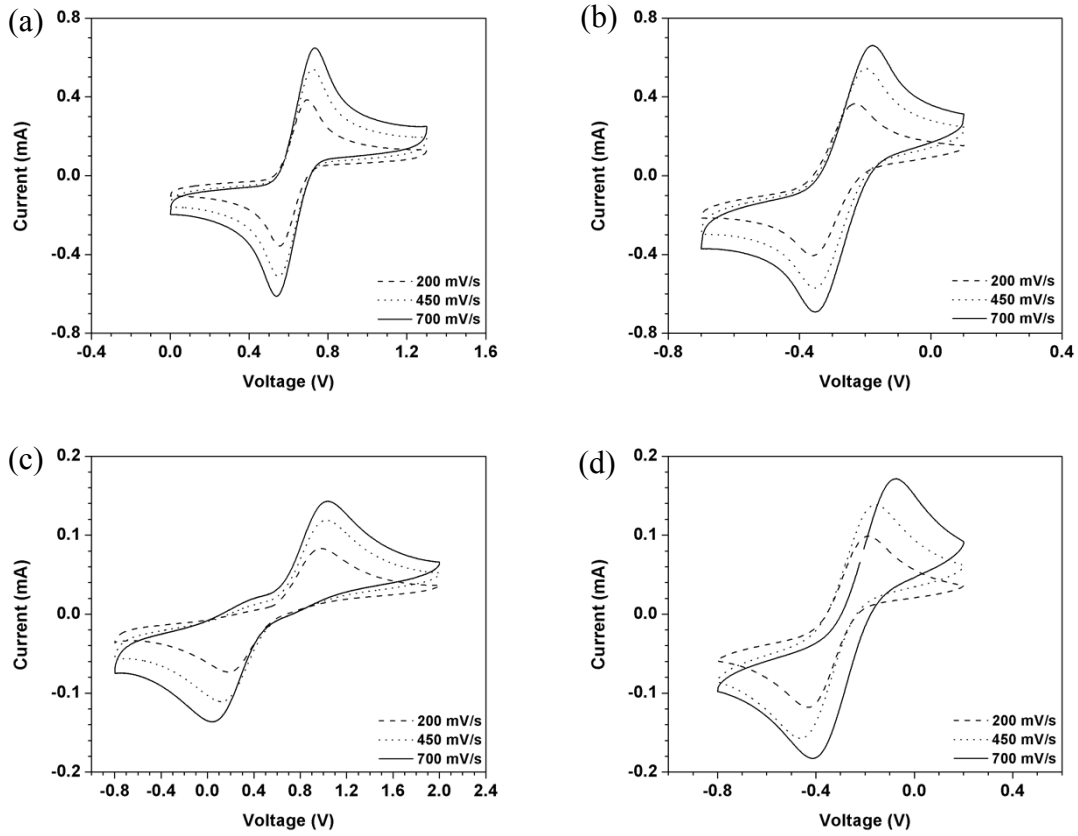

Figure S8: Voltammetric response of 2 cm^2 Pt and 1 cm^2 ITO electrodes in (a, c) 1 mM dmFc or (b, d) 1 mM $CoCp_2PF_6$ and 0.1 M TBATFB in PC at scan rates of 200, 450, and 700 mV s^{-1}. Diffusion coefficients are calculated from the slope of peak currents versus the square root of the scan rate. The increased peak separation of the voltammograms for the ITO electrodes is expressed in the lower heterogeneous rate constant of the redox systems for ITO.

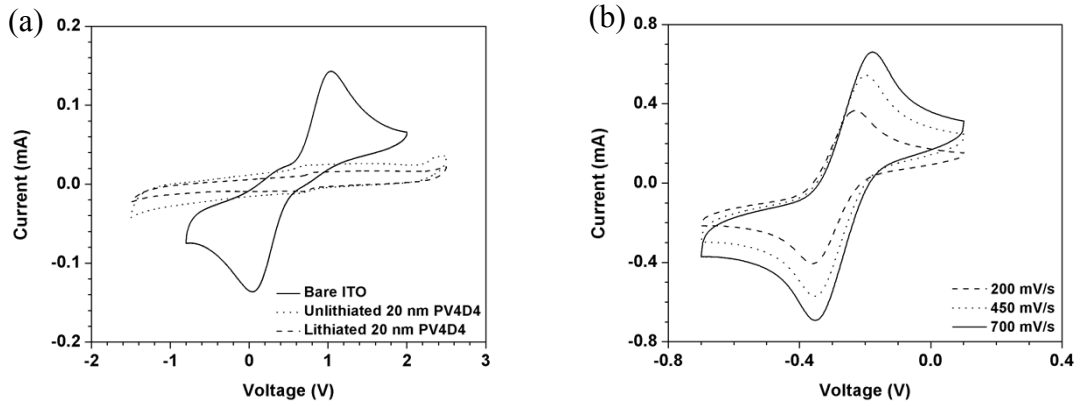

Figure S9: Voltammetric response of unlithiated and lithiated 20 nm PV4D4 films and ITO electrodes in (a) 1 mM dmFc or (b) 1 mM $CoCp_2PF_6$ and 0.1 M TBATFB in PC. The voltammetric responses of the PV4D4 films are stable across multiple sweeps for each scan rate; shown here are the third cycles at 700 mV s^{-1}. Peak currents used in the pinhole density calculations are the oxidation current plateaus at the redox potential (~0.75 V for dmFc and ~ -0.25V for $CoCp_2PF_6$). It is observed that the peak current for dmFc is appreciably larger in the μA range than $CoCp_2PF_6$ despite having a larger solvation shell diameter. The slope of the voltammograms is due to the electrolyte resistance of the electrochemical cell.

References

1. C. P. Rhodes, J. W. Long, M. S. Doescher, J. J. Fontanella and D. R. Rolison, *J. Phys. Chem. B*, 2004, **108**, 13079-13087.
2. S. R. Gowda, A. L. M. Reddy, M. M. Shaijumon, X. Zhan, L. Ci and P. M. Ajayan, *Nano Lett.* 2011, **11**, 101-106.
3. S. Zhang, J. Y. Lee and L. Hong, *J. Power Sources,* 2004, **134**, 95-102.
4. J. F. Ribeiro, R. Sousa, M. F. Silva, L. M. Goncalves, M. M. Silva and J. H. Correia, in *Batteries and Energy Technology*, Vol. 45 (Eds: S. Narayan, A. Manivannan, A. Manthiram), **2013**, 139.
5. Y.-C. Perng, J. Cho, S. Y. Sun, D. Membreno, N. Cirigliano, B. Dunn and J. P. Chang, *J. Mater. Chem. A* 2014, **2**, 9566-9573.
6. O. Chailapakul and R. M. Crooks, *Langmuir* 1995, **11**, 1329-1340.
7. R. Pyati and R. W. Murray, *J. Am. Chem. Soc.* 1996, **118**, 1743-1749.
8. E. I. Rogers, D. S. Silvester, D. L. Poole, L. Aldous, C. Hardacre and R. G. Compton, *J. Phys. Chem. C*, 2008, **112**, 2729-2735.
9. E. Sabatani and I. Rubinstein, *J. Phys. Chem.,* 1987, **91**, 6663-6669.
10. R. Feeney and S. P. Kounaves, *Electrochem. Commun.,* 1999, **1**, 453-458.
11. C. R. Cabrera and A. J. Bard, *J. Electroanal. Chem. Interfacial Electrochem.,* 1989, **273**, 147-160.
12. A. Lewandowski, L. Waligora and M. Galinski, *J. Solution Chem.,* 2013, **42**, 251-262.